

# Numerical Study of a High Head Francis Turbine with Measurements from the Francis-99 Project

**H. Wallimann and R. Neubauer**

Andritz Hydro AG, Hardstrasse 319, 8021 Zürich, Switzerland

E-mail: Henrik.Wallimann@andritz.com

**Abstract.** For the Francis-99 project initiated by the Norwegian University of Science and Technology (NTNU, Norway) and the Luleå University of Technology (LTU, Sweden) numerical flow simulation has been performed and the results compared to experimentally obtained data. The full machine including spiral casing, stay vanes, guide vanes, runner and draft tube was simulated transient for three operating points defined by the Francis-99 organisers. Two sets of results were created with differing time steps. Additionally, a reduced domain was simulated in a stationary manner to create a complete cut along constant prototype head and constant prototype discharge. The efficiency values and shape of the curves have been investigated and compared to the experimental data. Special attention has been given to rotor stator interaction (RSI). Signals from several probes and their counterpart in the simulation have been processed to evaluate the pressure fluctuations occurring due to the RSI. The direct comparison of the hydraulic efficiency obtained by the full machine simulation compared to the experimental data showed no improvement when using a  $1^\circ$  time step compared to a coarser  $2^\circ$  time step. At the BEP the  $2^\circ$  time step even showed a slightly better result with an absolute deviation 1.08% compared with 1.24% for the  $1^\circ$  time step. At the other two operating points the simulation results were practically identical but fell short of predicting the measured values. The RSI evaluation was done using the results of the  $2^\circ$  time step simulation, which proved to be an adequate setting to reproduce pressure signals with peaks at the correct frequencies. The simulation results showed the highest amplitudes in the vaneless space at the BEP operating point at a location different from the probe measurements available. This implies that not only the radial distance, but the shape of the vaneless space influences the RSI.

## 1. Introduction

Computational fluid dynamics (CFD) is an established tool in industry for the design of Francis and other types of turbines. The history of numerical flow simulation is illustrated in [1]. Continuous effort is needed to improve and validate the CFD tools. The principle task of the CFD tools is to predict the hydraulic efficiency and pressure distribution as accurately as possible and capture flow phenomena of importance. The interaction between stationary and rotary parts is an important phenomena of the hydraulic system. It is a source of vibration that can lead to serious damage to the machine [2]. Predictions for low part load and high load away from the best efficiency points gain in importance due to the increasing demand to operate a turbine with flexible power output.

The Francis-99 project offers an opportunity to test the state of the art tools available today. It also allows assessing CFD setups that are not yet integrated in the day to day business as computational



time and resources are often prohibitive, but might become part of the standard design procedure in the near future. The measurements provided by the organizers of the Francis-99 project exceed the data produced during a model test and allow a more detailed comparison between experimental and numerical values.

Similar studies have been performed in the past for pump turbines in turbine mode, for example in [3] and [4]. In these studies, the SST turbulence model was found to cope best with the pressure fluctuations due to RSI and was consequently used again for this study.

In this paper the results of CFD simulations of the full machine and a reduced domain are presented. The hydraulic efficiency is compared qualitatively and quantitatively. The results of the full machine simulations are compared with data from several pressure probes installed at the measured model and the pressure fluctuations due to RSI are discussed.

## 2. Experimental Model

The experimental values used for comparison and validation in this paper were obtained at the test rig at the Waterpower laboratory, NTNU in Norway. For the discussed operation points, the test rig was operated in an open loop manner with the draft tube connected to a downstream tank open to air. A more detailed description of the test rig and instrumentation can be found in [5]. The tested model was designed based on the prototype values of the Tokke power plant in Norway. The corresponding prototype values are  $H_p=377\text{m}$ ,  $P_p=110\text{MW}$ ,  $D_p=1.779\text{m}$  and  $Q_p=31\text{m}^3/\text{s}$ .

The diameter of the model is  $D_M=0.349\text{m}$  (scale = 1:5.1). The model runner consists of 15 full length and 15 splitter blades. The number of guide vanes is 28. Experimentally the best efficiency point was found at a  $H_M=11.91$ ,  $Q_M=0.203\text{m}^3/\text{s}$  and a runner speed of  $n_M=5.59\text{rev/s}$ . It amounts to  $\eta_M=92.61\%$ . A list of the provided operating point data is shown in Table 1.

	flow rate [m <sup>3</sup> /s]	net head [m]	guide vane angle [°]	Runner angular speed [rev/s]	Efficiency [%]
part load	0.071	12.29	3.91	6.77	71.69
BEP	0.203	11.91	9.84	5.59	92.61
high load	0.221	11.84	12.44	6.16	90.66

**Table 1.** Experimental operating point data for part load, BEP (best efficiency point) and full load

## 3. Numerical Model:

### 3.1. Full Machine

To numerically simulate the experimentally investigated model the commercial software Ansys CFX, solver version 14.0, was used. The numerical grid was created with ICEM CFD using the ICEM files offered by the Francis-99 organizers. The complete machine consisted of a grid combining spiral casing, stay vanes and guide vanes (different for each operating point), a second grid representing the runner and a third grid containing the draft tube. The number of nodes was 3.6mio, 5.9mio and 3.6mio respectively. This added up to a total of 13.1mio nodes. A grid sensitivity test performed in [5] for the BEP showed a similar number of nodes to be a reasonable resolution. Except for merging two separately provided runner parts (runner with blades and part just below the hub) and improvement of the geometric match of the interface between the guide vanes and the runner, no changes were made to the provided grids. Figure 1 shows a picture of the complete domain.

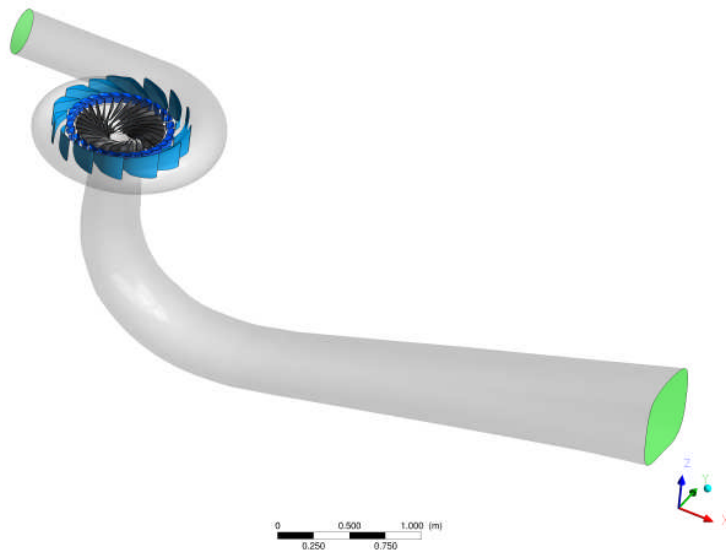


**Figure 1. Computational domain of full machine including spiral casing, stay vanes, guide vanes, runner and draft tube**

The shear stress transport (SST) model was chosen for turbulence modelling. The high resolution scheme was used as advection scheme and for the turbulence numerics first order was chosen. The transient scheme was set to second order backward Euler.

At the spiral casing inlet the discharge of the operating point was imposed as boundary condition. The draft tube outlet was modelled as outlet with an average pressure of 1bar, representing the open loop setup of the model test rig. The interfaces between guide vanes and runner as well as runner and draft tube were modelled as transient interfaces covering the full 360°. All walls were modelled as hydraulically smooth. A first set of three simulations was started without initial solution and run for five revolutions. The time step was set for each operating point individually, depending on the runner speed, to result in a step of 2° in respect to the runner rotation. A second set of simulations was run with a time step corresponding to a 1° angular step using the 2° results as initial condition and run for two more revolutions.

Monitor points were set to represent the pressure probes used during the experimental investigation. A Fortran routine was integrated to conduct a discrete Fourier transformation on the last revolution and store the amplitudes of the first three harmonics. For the rotating runner domain the first harmonic was chosen according to the guide vane passing frequency (28 per revolution) and for the stationary domains the first harmonic was chosen based on the number of blades with full length (15). Other numerical results as e.g. efficiency were recorded and averaged over the last revolution of the simulation.

Simulations were performed for the three given operation points; one in part load operation, one at the experimentally found best efficiency point and one at high load operation according to the provided grids.

### 3.2. Reduced Domain

A second numerical setup was used to evaluate the qualitative prediction of the hydraulic efficiency. The domain was reduced to the runner, simulating a single channel including one full length blade and one splitter blade as well as periodic surfaces by adjusting the provided ICEM CFD files. A discharge boundary condition was used and the operating point fully defined by setting an inflow angle representing the flow coming from the guide vanes. As for the full domain the SST model was used for turbulence modelling as well as first order for turbulence numerics. For the advection scheme a blend factor of 1.0 was used, enforcing second order accuracy.

Steady state simulations were performed for the 3 given operating points as well as for a constant prototype H cut near  $H_p=386.9\text{m}$  and a constant Q cut  $Q_p=30.06\text{m}^3/\text{s}$  which correspond to the found BEP by the model test and transposed to prototype values by hydraulic similitude according to IEC 60193 [6].

## 4. Results

### 4.1. Hydraulic Efficiencies: Full Machine

Figure 2 shows the experimentally obtained hydraulic efficiency compared to the efficiencies calculated from the CFD simulation of the full machine. Although the values are plotted against model discharge, the three operating points have to be regarded as individual points on the hill chart and do not represent a cut along a constant head. The CFD value is the average taken over the last revolution. Generally the CFD predictions should be slightly too high as no leakage losses through the labyrinth gaps can occur and no disc friction is present. As can be seen from the figure, the BEP of the simulation with a  $2^\circ$  step matches best with a deviation of 1.08%. The  $1^\circ$  time step simulation results in a slightly higher efficiency, with a deviation of 1.24%. The high load point at a model discharge of  $0.221\text{m}^3/\text{s}$  is similarly over predicted by both settings (+3.6%) as well as the efficiency at the part load operating point (+11.0%).

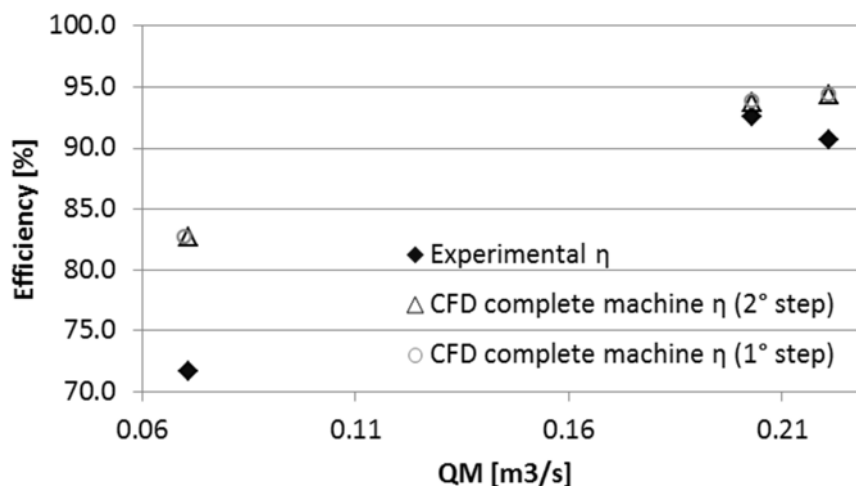


Figure 2. Comparison of experimental and CFD predicted efficiency simulating the complete machine

### 4.2. Hydraulic Efficiencies: Reduced Domain

Figure 3 shows the comparison of the three operating points plotted over the discharge in model scale. Due to the reduced domain the absolute values cannot be compared but only the qualitative distribution. Although it looks like the BEP was correctly predicted, a look at Figure 4 showing the circumferential velocity reveals that the simulated operating point is a high load operating point. The negative circumferential values indicate swirl in counter rotating direction. The CFD BEP is located at lower discharges (dashed curve representing the CFD BEP of Figure 5), where the swirl tends to zero.

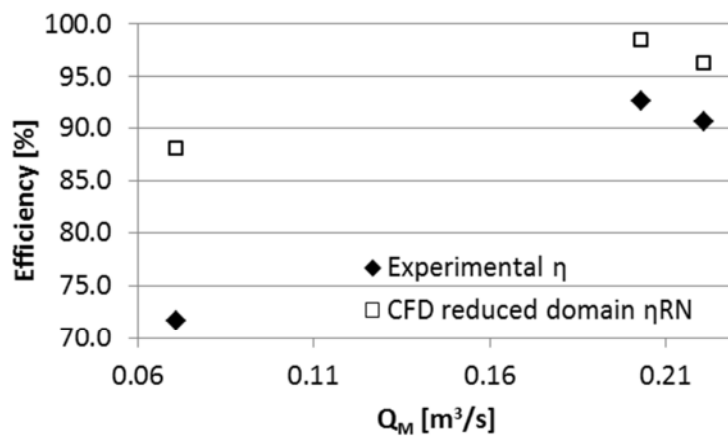


Figure 3. Qualitative comparison of experimental and CFD predicted efficiency simulating a reduced domain

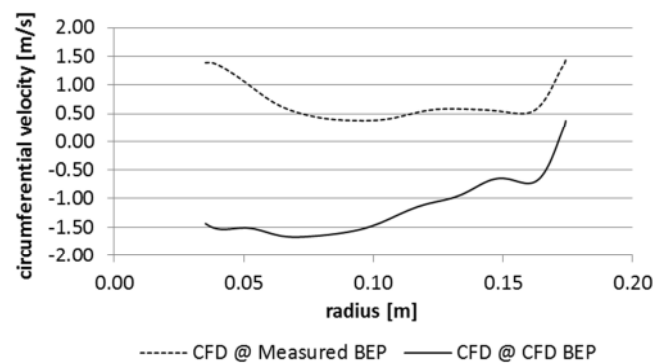


Figure 4. Circumferential velocities at runner outlet of CFD reduced domain simulation

The following figures (Figure 5 and Figure 6) show a cut at constant prototype head or prototype discharge. For a given prototype diameter of 1.779m and a rotational speed of 375rpm the prototype BEP derived from the measured BEP would be at a net head of 386.9m and a discharge of 30.1m³/s. Therefore the cuts were made at these values. The peak of the efficiency curve is shifted to lower discharge. This is often observed for low specific speed runners as the guide vane losses are not included and don't increase linear with increasing discharge. The curve over H is very flat and the measured and transposed BEP is located at the plateau.

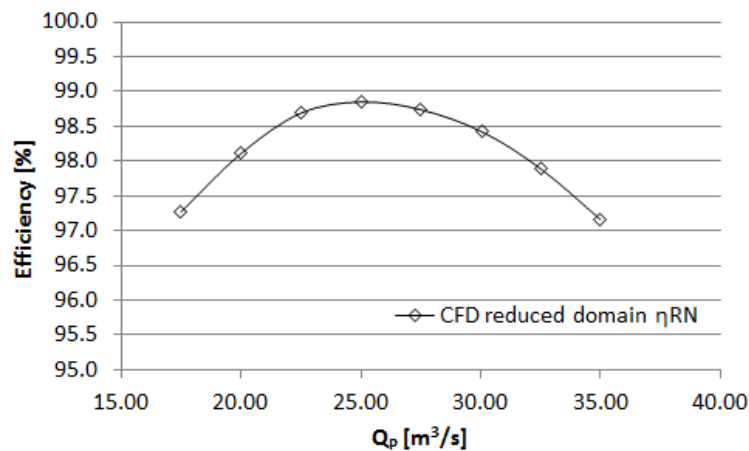


Figure 5. CFD reduced domain simulation predicted runner efficiency at constant prototype net head of 386.9m

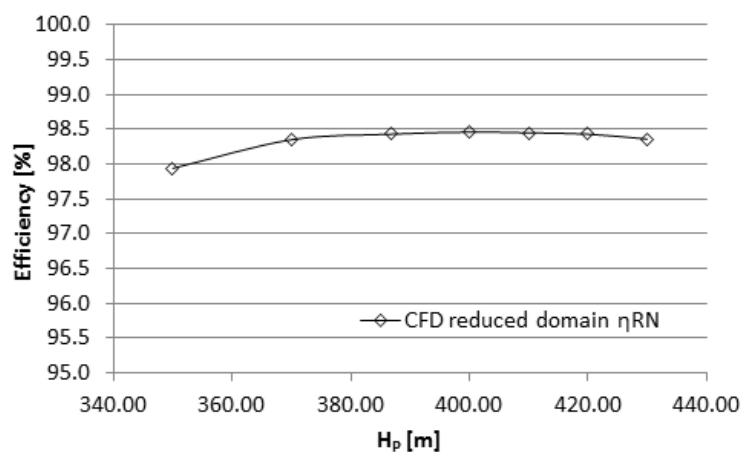


Figure 6. CFD reduced domain predicted runner efficiency at constant prototype discharge of 30.1m³/s

#### 4.3. Rotor Stator Interaction

The three operating points (part load, BEP and high load) simulated with a 2° step have been evaluated in respect to pressure amplitudes originating from the interaction between the rotary and stationary components. Table 2 shows an overview of the results. The top three rows indicate the geometric parameters influencing the RSI. Changing the guide vane angle leads to a different extension of the vaneless space from the trailing edge of the guide vanes (TE) to the leading edge of the runner blades (LE). The minimum radial distance is reached at high load.

Figure 7 shows the top view of the 3D geometry. A circular plane of evaluation has been created to evaluate the area average of the pressure amplitudes in the vaneless space. The radius of the area has been chosen so that the surface includes the location of pressure probe VL01. The probe position is indicated by a pink sphere. All frequencies have been normalized by the runner frequency  $f_{RN}$ .

location	variable	normalized frequency	unit	part load	BEP	high load
guide vanes	guide vane angle	-	[°]	3.91	9.84	12.44
	radial distance between		[mm]	24	19	17
vaneless space	guide vane TE and runner blade LE	-	[%D <sub>M</sub> ]	6.9	5.5	4.9
vaneless space	area averaged amplitude	$f/f_{RN} = 30$	[kPa]	0.859	1.555	1.312
stay vane surface	maximum amplitude	$f/f_{RN} = 30$	[kPa]	0.364	0.408	1.141
guide vane surface	maximum amplitude	$f/f_{RN} = 30$	[kPa]	0.999	2.377	1.829
runner blades surface	maximum amplitude	$f/f_{RN} = 28$	[kPa]	2.161	5.448	3.834
runner blade 4	maximum amplitude	$f/f_{RN} = 28$	[kPa]	2.137	5.218	3.757
draft tube surface	maximum amplitude	$f/f_{RN} = 15$	[kPa]	0.744	0.278	0.234
draft tube surface	maximum amplitude	$f/f_{RN} = 30$	[kPa]	0.470	0.219	0.198

Table 2. RSI Evaluation

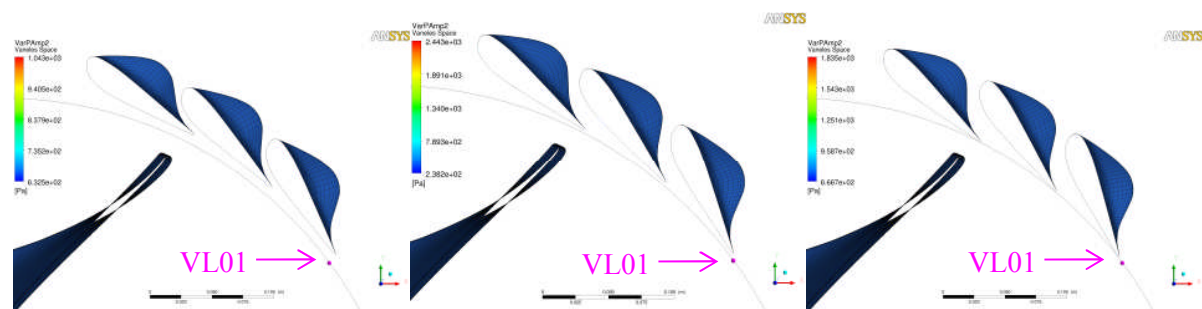
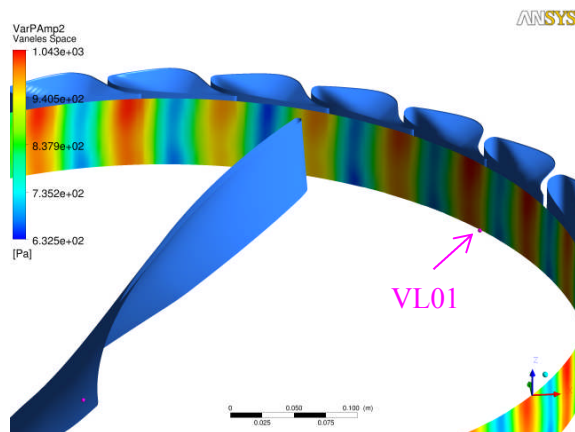


Figure 7. Top view of vaneless space for part, BEP and high load (left to right)

The distribution of pressure amplitudes for the different operating points on the circular evaluation surface is shown by Figure 8, Figure 9 and Figure 10. The area averaged pressure amplitudes are 0.859kPa, 1.555kPa and 1.312kPa for part, BEP and high load. These values show that the strongest interaction is to be expected at the BEP. It implies that not only the radial distance from the trailing edge of the guide vane to the leading edge of the passing runner blade, but the shape of the vaneless space is of importance. The larger the guide vane angle the smaller the radial distance, but at the same time the distance between guide vane trailing edge and the surface of the adjacent guide vane is increased. The pressure amplitude distribution shows a circumferential pattern. Part load operation and BEP operation show a similar pattern with the high amplitude patches moving with the rotational movement of the guide vanes. High load operation shows high amplitude patches that are split up.

The overall maximum amplitude value on the runner blades surface is found at the BEP and amounts to 5.448kPa. The maximum amplitude for the guide vanes is also found at the BEP. The stay vanes experience amplitudes reduced up to 83% compared to the guide vane values. The maximum value appears at the high load operating point. For the draft tube the maximum values for two harmonics are listed in Table 2 as the splitter blades are shortened and the first harmonic of 15 (normalized frequency) shows slightly higher amplitudes than the second harmonic of 30. The highest amplitude of 0.744kPa is found at the part load operating point for the first harmonic. High load shows the lowest amplitudes in the draft tube cone.



**Figure 8. Distribution of pressure amplitudes in vaneless space at part load**

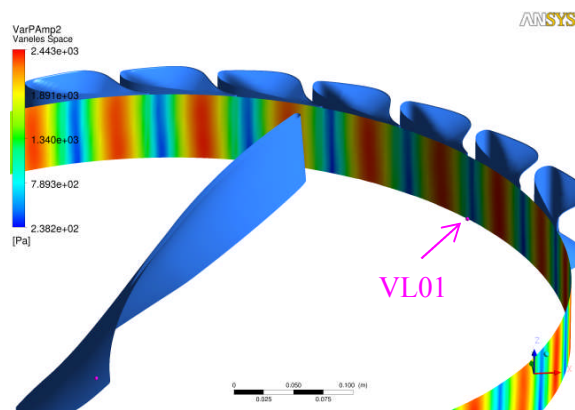


**Figure 9. Distribution of pressure amplitudes in vaneless space at BEP**

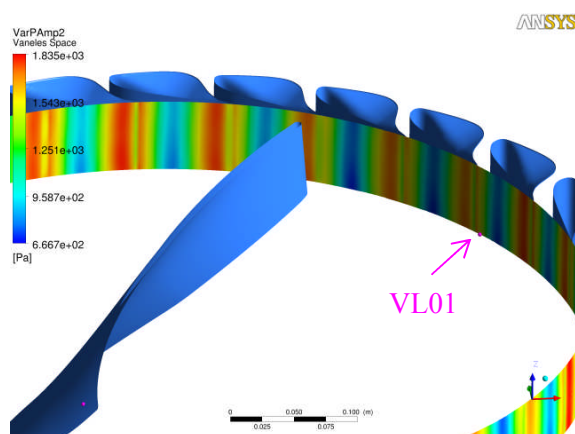


**Figure 10. Distribution of pressure amplitudes in vaneless space at high load**

To compare CFD and experimental values the CFD pressure signal at the location of pressure probe VL01 has been extracted. Both signals were processed by a discrete Fourier transformation. The complete experimental signal was used as input whereas of the CFD data the last revolution was used.

Below, in Figure 11, the pressure amplitudes are plotted versus the frequency normalized by the runner frequency. For better visibility the amplitude spectra have been plotted separately. As can be seen both, experimental and CFD signals, show peaks at 15 and 30 times the runner frequency which corresponds to the first and second harmonic of the runner blade passing frequency. In part and high



load a small peak at 60 times the runner frequency is indicated as well. The peak of the experimental signal at the BEP near 17.9 and at high load near 16.2 times the runner frequency (100Hz) was identified as system excitation frequency in [5] and therefore not present in the CFD signal.

Quantitatively the pressure probe signal shows the maximum amplitude in the vaneless space at the high load operating point. Figure 8 to Figure 10 indicate the location of pressure probe VL01 as pink sphere and reveal that the amplitude is dependent on the spatial position and the overall maximum amplitude in the vaneless space is at BEP operating conditions.

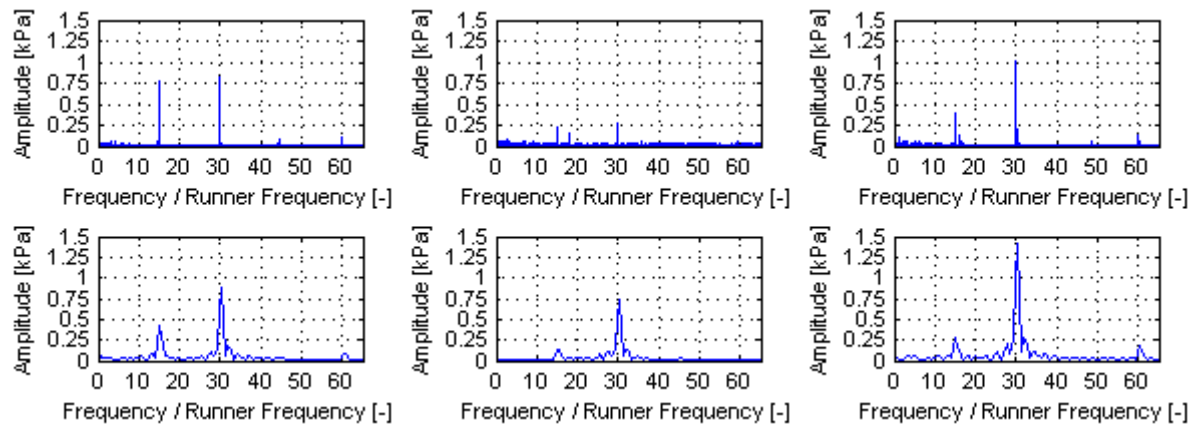


**Figure 11. Comparison of experimental (top) and CFD (bottom) amplitudes spectrum of sensor VL01 for part, BEP and high load (from left to right)**

Figure 12 shows the pressure side of runner blade 4, where the pressure probes P42 and P71 (near trailing edge) are mounted. The pressure amplitudes are shown for the BEP and correspond to the guide vane passing frequency of 28 per runner revolution. The amplitude values for P42 and P71 are 0.648kPa and 0.309kPa respectively. Figure 13 shows the suction side of the same blade. The maximum pressure amplitude for the chosen blade is 5.218kPa and occurs at the leading edge surface coming closest to the guide vane trailing edges. On the pressure side the amplitudes first decrease and then increase slightly again when moving downstream along the blade. On the suction side the amplitudes gradually become smaller towards the trailing edge.

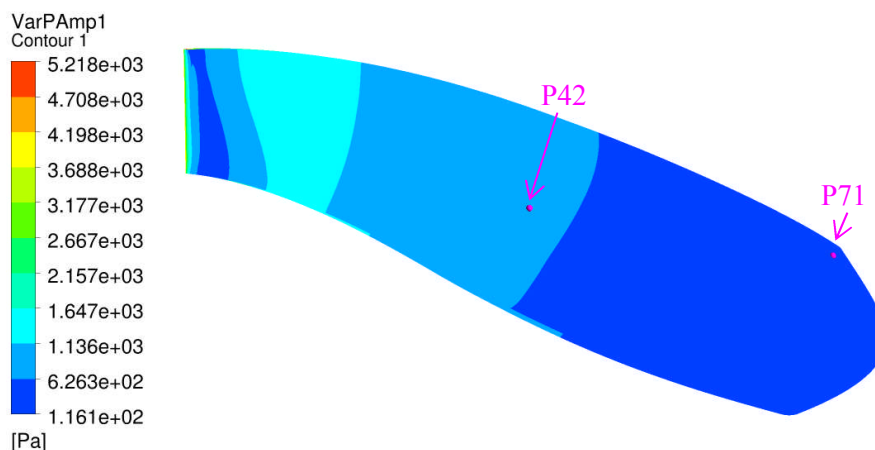


**Figure 12. Pressure amplitude distribution on runner blade 4 pressure side at BEP**

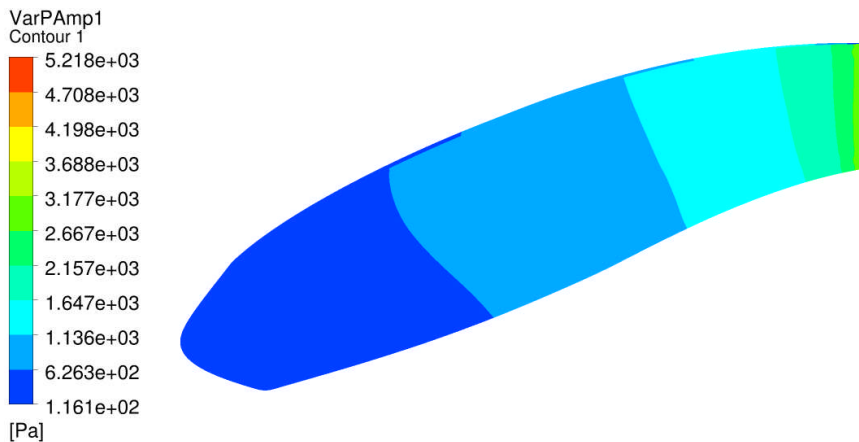
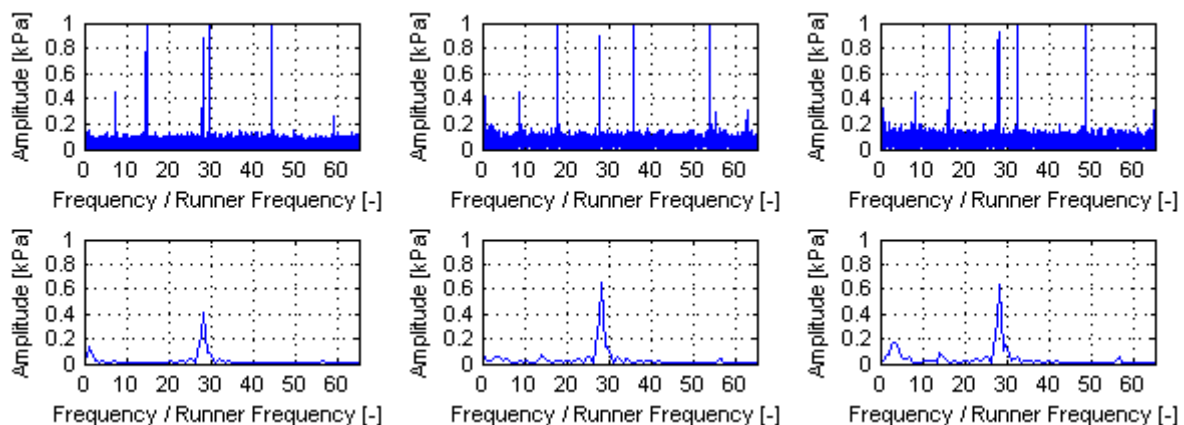


**Figure 13. Pressure amplitude distribution on runner blade 4 suction side at BEP**

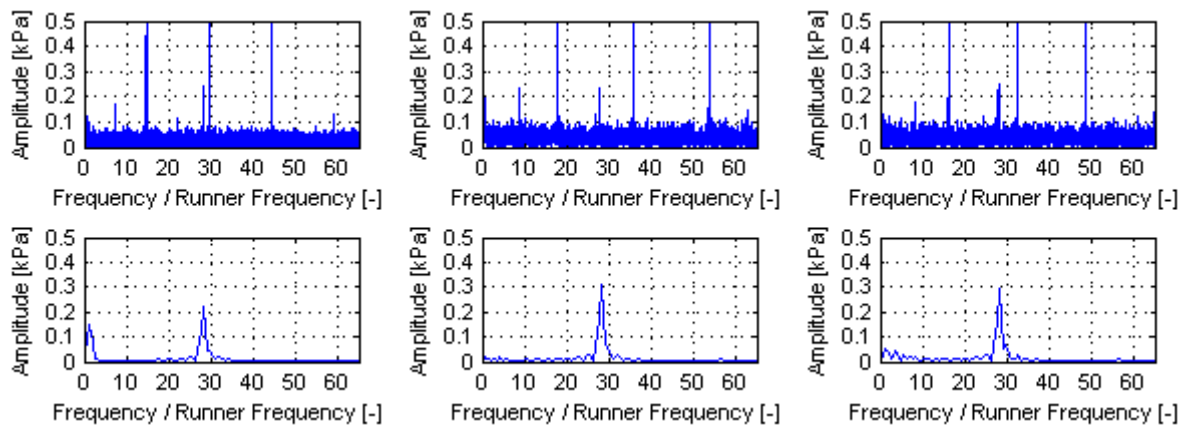
The following figures (Figure 14 to Figure 16) show the pressure amplitudes of experimental and CFD signals of all the blade mounted probes: P42 and P71 on the pressure side and S51 on the suction side. As for the VL01 sensor amplitudes the experimental data shows several peaks not observed in the CFD results. There are 4 peaks in each graph that change position depending on the runner frequency. The grid frequency is 50Hz and appears between a normalized frequency of 7.4 to 8.9. The three large peaks are observed system excitation frequencies 100Hz, 200Hz and 300Hz [5].

The normalized frequency of interest for comparison is the guide vane passing frequency which is 28 and captured by all signals. As already seen from the amplitude distribution across the blade, P71 shows much lower amplitudes than P42 located more upstream. Note, that the y-axis is adjusted for each sensor. The CFD signals show lower amplitudes at part load for all sensors compared to BEP and high load, which are close to equal. The experimental signals do not show a variation across the operating points, suggesting that amplitude of the oscillation downstream the blade surface is not influenced anymore due to the guide vane position, but only the oscillation frequency is triggered by the interaction.

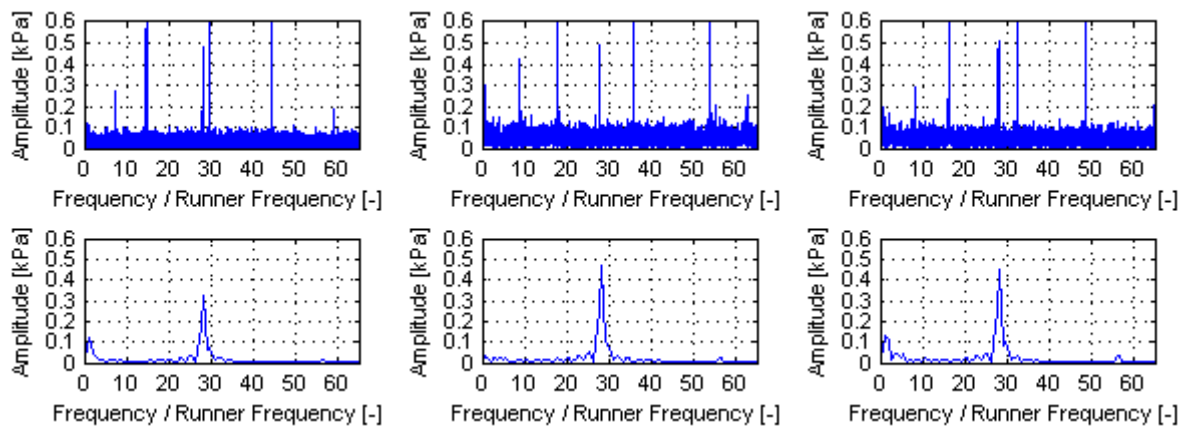
Experimental and CFD value agree on the tendency of the value when comparing each sensor for a given operating point. For the BEP operating point P42 experiences the largest oscillation with an amplitude of 0.904kPa, P71 an amplitude of 0.236kPa and S51 an amplitude of 0.494kPa. The corresponding CFD values are 0.648kPa, 0.309kPa and 0.469kPa respectively.



**Figure 14. Comparison of experimental (top) and CFD (bottom) amplitudes spectrum of sensor P42 for part, BEP and high load (from left to right)**



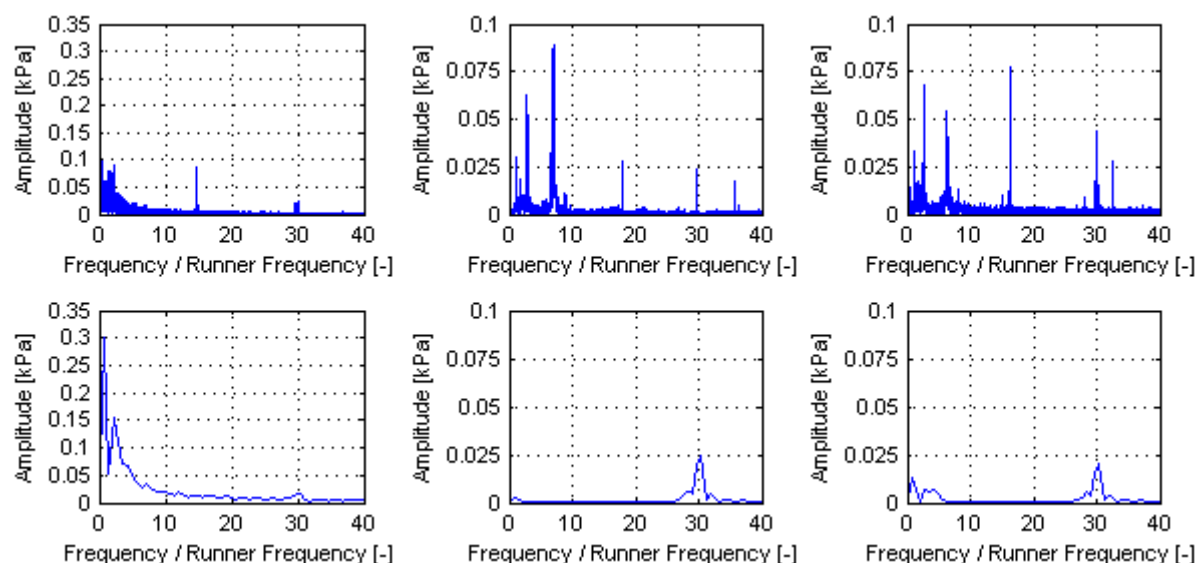
**Figure 15.** Comparison of experimental (top) and CFD (bottom) amplitudes spectrum of sensor P71 for part, BEP and high load (from left to right)



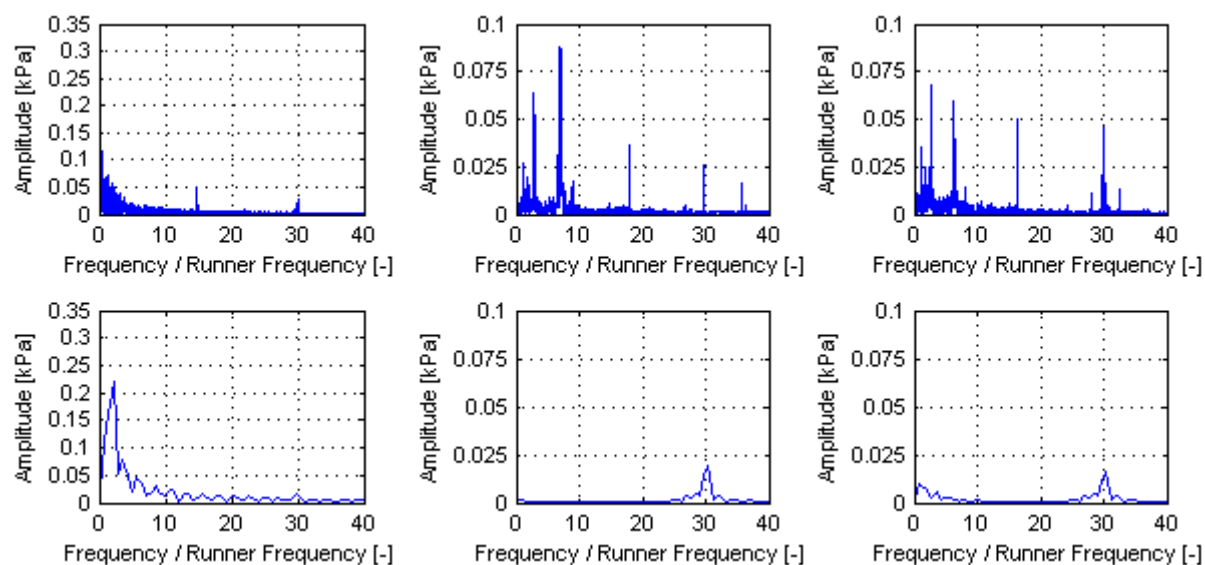
**Figure 16.** Comparison of experimental (top) and CFD (bottom) amplitudes spectrum of sensor S51 for part, BEP and high load (from left to right)

Figure 17 and Figure 18 compare the amplitude spectra of the sensors installed in the draft tube cone. Both sensors are at the same height, but they are rotated by  $30^\circ$  around the rotational axis of the turbine so that DT11 is closer to the outer and DT21 closer to the inner bend of the draft tube. Therefore an asymmetry in the signals is expected. The single peak between 10 and 30 in all six experimental signals is again the above mentioned 100Hz excitation frequency.

At the BEP, the amplitude at a normalized frequency of 30 matches very well for DT11 and DT21. The CFD shows no low frequencies as no vortex is present. For part load, low frequencies originating from a part load vortex appear in both experimental and CFD signals. The CFD amplitudes over predict the effect of the vortex. The runner passing frequency is barely present anymore. At high load, contrary to the CFD amplitudes for the runner passing frequency the experimental values show an increase compared to the BEP.



**Figure 17.** Comparison of experimental (top) and CFD (bottom) amplitudes spectrum of sensor DT11 for part, BEP and high load (from left to right)



**Figure 18.** Comparison of experimental (top) and CFD (bottom) amplitudes spectrum of sensor DT21 for part, BEP and high load (from left to right)

## 5. Conclusion

Transient simulations have been conducted to compare with experimental data provided by the organisers of the Francis-99 project. The best match of hydraulic efficiencies was found at the BEP with a +1.08% deviation from the experimental value. Larger deviations were found at part and high load. No improvement was observed when using a  $1^\circ$  time step instead of a  $2^\circ$  time step. The  $1^\circ$  time step showed a worse match at the BEP (+1.24%) and identical values for the part load (+11.0%) and high load operating point (+3.6%).

The efficiency results shows that CFD is not yet suitable to predict absolute efficiency values away from the best efficiency point and further improvements have to be made. Possible errors are the accuracy of the geometry, grid dependent effects as well as modelling. It would be interesting to compare the discharge boundary condition used with a total pressure boundary condition. Further, it was shown that with a reduced domain simulation it is possible to predict the shape of the efficiency curve except for a shift to lower discharges.

Detailed analysis of the pressure amplitudes in the vaneless space showed a maximum average amplitude of 1.555kPa at the BEP. The pressure probe installed in the vaneless space showed the maximum amplitude for the high load operating point. Due to the spatial distribution of the pressure amplitudes this was found to be only a local maximum. The result suggests that the shape of the vaneless space and not only the minimal distance between guide vane trailing edge and runner blade leading edge influence the pressure amplitudes occurring due to RSI.

Comparison of the amplitude spectrum between measured and simulated pressure signals showed that CFD captures the relevant frequencies. The tendency of the amplitude values was correct for the probe in the vaneless space and when comparing the sensors on the blade for a given operating point. The comparison of the signals in the draft tube cone compared well for the runner passing frequency but fell short of the experimental values for low frequencies associated with a part or full load vortex. To improve the quality of the CFD results concerning the absolute amplitude values, further effort is needed.

## 6. Acknowledgements

The authors would like to thank the organisers of the Francis-99 project for the opportunity to participate in this project and test the state of the art CFD tools.

## References

- [1] Keck H, Sick M 2008 *Thirty years of numerical flow simulation in hydraulic turbomachines* Acta Mech **211** pp 211-229
- [2] Egusquiza E, Mateos B, Escaler X 2002 *Analysis of Runner-Stator Interaction in Operating Pump-Turbines* Proceedings of the 21<sup>st</sup> IAHR Symposium on Hydraulic Machinery and Systems, Lausanne, Switzerland
- [3] Keller M, Doerfler P, Sallaberger M, Sick M 2005 *Rotor-Stator Interaction in Pump Turbines – Numerical Prediction and Experiment* Proceedings of Hydro2005 Villach Austria
- [4] Liang Q W, Keller M, Sick M 2009 *Rotor Stator Interaction during no Load Operation of Pump Turbines* Proceedings of Hydro2009 Lyon France
- [5] Trivedi C, Cervantes J M, Gandhi B K, Dahlhaug O G 2013 *Experimental and Numerical Studies for a High Head Francis Turbine at Several Operating Points* ASME J. of Fluids Engineering **135** 111102
- [6] IEC 60193 1999-11 IEC *Hydraulic Turbines, Storage Pumps and Pump-Turbines – Model acceptance tests* International Electrotechnical Commission